Global Journal of Science Frontier Research: F
Mathematics and Decision Sciences
Volume 16 Issue 6 Version 1.0 Year 2016
Type : Double Blind Peer Reviewed International Research Journal
Publisher: Global Journals Inc. (USA)
Online ISSN: 2249-4626 & Print ISSN: 0975-5896

On the Role of Luminal Flow and Interstrut Distance in Modelling Drug Transport from Half-Embedded Drug-Eluting Stent

By Akash Pradip Mandal & Prashanta Kumar Mandal
Visva-Bharati University

Abstract- A model for investigating the transport of drug from a half-embedded drug-eluting stent (DES) is developed. Keeping the relevance of the physiological situation in view, the luminal drug transport is considered as an unsteady convection-diffusion process, while the drug transport within the arterial tissue is supposed to commence as a diffusion process. The Marker and Cell (MAC) method has been used to handle numerically the governing equations of motion for the luminal flow and the drug transport through the lumen and the tissue. The effects of quantities of significance such as Reynolds number (Re), Womersley number (α) and interstrut distance on the transport of drug through both the lumen and the tissue are quantitatively investigated. Our simulation predicts that the mean concentration of drug increases with the decreases of Reynolds number and with an increase in the Womersley number.

Keywords: embedded drug-eluting stent; flow pulsatility; interstrut distance; convection; womersley number.

GJSFR-F Classification: MSC 2010: 00A05

Strictly as per the compliance and regulations of :

On the Role of Luminal Flow and Interstrut Distance in Modelling Drug Transport from Half-Embedded Drug-Eluting Stent

Akash Pradip Mandal [α] & Prashanta Kumar Mandal [σ]

Abstract- A model for investigating the transport of drug from a half-embedded drug-eluting stent (DES) is developed. Keeping the relevance of the physiological situation in view, the luminal drug transport is considered as an unsteady convection-diffusion process, while the drug transport within the arterial tissue is supposed to commence as a diffusion process. The Marker and Cell (MAC) method has been used to handle numerically the governing equations of motion for the luminal flow and the drug transport through the lumen and the tissue. The effects of quantities of significance such as Reynolds number (Re), Womersley number (α) and interstrut distance on the transport of drug through both the lumen and the tissue are quantitatively investigated. Our simulation predicts that the mean concentration of drug increases with the decreases of Reynolds number and with an increase in the Womersley number. The present results also predict a single peak profile of drug concentration when the pair of struts are placed one-half strut width and also as the interstrut distance increases, distinct peaks form over each strut.

Keywords: embedded drug-eluting stent; flow pulsatility; interstrut distance; convection; womersley number.

I. Introduction

Atherosclerosis is a disease that affects coronary, carotid and other peripheral arteries in the body. Coronary artery disease (CAD) pertains to a blockage or narrowing of coronary arteries. Once detected as such, there are a number of interventional ways to alleviate a stenosis in a coronary artery. Drug-eluting stents have drastically reduced the rate of in-stent restenosis compared to bare-metal stents (BMS^s) viz. 8.9% after eight months compared to 36.6% for BMS in the same study [35] and have since become the most choice for treatment of coronary arteries afflicted with advanced atherosclerotic lesions [34]. The success of DES is usually associated with the effective local delivery of potent therapeutics to the target site with programmed pharmocokinetics. The local drug concentrations achieved are directly correlated with the biological effects and local toxicity, and establishing the optimum dose to be delivered to the tissue remains a challenge in DES design and manufacturing [3, 11, 32]. The association of tissue prolapse (i.e. the deflection of the tissue between the struts of the stent) and in-stent thrombosis has also been reported in several studies [30, 27, 9]. Some researchers [13, 16, 5] are on the opinion that platelet activation, endothelium injury and inadequate antiplatelet therapy plays an important role for in-stent thrombosis. A number of experimental and numerical studies on DES have been carried out in recent past to address the issues like its efficiency and safety [4, 18, 2, 6, 21, 28, 29, 31, 22].

McGinty et al. [20] have included the layer structure of the arterial wall into their 1D studies. Zunino et al. [36] opined that model based on dimension reduction enable a comprehensive

Author: Department of Mathematics, Visva-Bharati University, Santiniketan-731235, West Bengal, India. e-mail: pkmind02@yahoo.co.uk

geometrical and physical description of stenting at affordable computational costs. Kolachalama et al. [14, 15] studied the impact of luminal flow on the drug transport from DES and they concluded that the use of DES requires a complex calculus that balances vascular and stent geometry as well as luminal flow. They showed that the flow imposes recirculation zones distal and proximal to the stent strut that extends the coverage of tissue absorption of eluted drug and induce asymmetry in drug distribution within the arterial tissue. Balakrishnan et al. [1] studied the coupled computational fluid dynamics and drug transport model in an idealised stented artery to predict drug deposition in single and overlapping DES and showed that the drug deposition appeared not only beneath regions of arterial contact with the strut but also beneath stagnant drug pools created by the separation flow. Hwang et al. [12] investigated the behaviour of hydrophobic and hydrophilic drugs as a convection-diffusion process and showed that the asymmetric strut distribution has a higher effect on hydrophilic drug distribution in comparison with hydrophobic one. Gogineni et al. [7] compared various stent geometries in order to determine most hemodynamically favourable stent. Models with multiple struts have also been developed to study the impact of different strut configurations and diffusivities on arterial drug distribution [2, 3, 8, 24, 25, 33]. Moreover, as the impact of flow pulsatility on arterial drug uptake is being increasingly characterised, several factors associated with the pulsatile nature of blood flow on arterial drug deposition have not been fully understood [26].

In an effort to better understand the validity and applicability of model assumptions, the present *in silico* investigation deals with the transport of drug from a half-embedded DES. This model is believed to be an extension of our previous model [19]. Here, we study the importance of flow pulsatility and interstrut distance on the drug transport within the framework of coupled computational fluid dynamics and mass transfer model. The governing equations of motion of unsteady momentum and mass transfer are successfully solved numerically by MAC method primarily introduced by Harlow and Welch [10]. The primary objective of the present study is to explore the effects of essential issues like Reynolds number, flow pulsatility, interstrut distance as well on the wall shear stress, the luminal drug concentration and the drug concentration within the arterial tissue by using relatively simple finite difference scheme in rather complex geometries. The novelty of the study lies in the inclusion of strut embedment and flow pulsatility on the unsteady distribution of both the mass and momentum transport. In this investigation, embedment of the strut in the arterial wall is assumed to be 50% only as the effect of embedment reveals only the change in magnitude of drug concentration by keeping the overall behaviour and the conclusions drawn unaltered [2].

II. Materials and Methods

a) Model geometry

The computational domain consists of a long axial arterial section of length L idealised as a rectangle where the embedded struts are assumed to be circular. The arterial wall thickness is taken to be 5 times of strut diameter (d) and the lumen to be 15-fold wide (cf. Figure 1). The size of strut and interstrut distance are adapted from the geometry introduced by Mongrain et al. [24]. We define a therapeutic zone for drug delivery consisting of a pair of half-embedded struts together with the upstream length (z_0) and the downstream length (z_l). All the simulation results are for this domain.

b) Dimensionless governing equations and boundary conditions

The streaming blood is assumed to be unsteady and Newtonian past a two-dimensional axi-symmetric stented artery and is thus governed by the time-dependent Navier-Stokes equations whose forms are as

Ref

12. Hwang CW, Wu D, Edelman ER (2001) Physiological transport forces govern drug distribution for stent-based delivery. Circulation 104:600–605

$$\frac{\partial w}{\partial t}+\left[\frac{\partial}{\partial r}(uw)+\frac{\partial}{\partial z}(w^2)+\frac{uw}{r}\right]\epsilon^8 = -\frac{\partial p}{\partial z}+\frac{\epsilon^7}{Re}\left(\frac{\partial^2 w}{\partial r^2}+\frac{1}{r}\frac{\partial w}{\partial r}+\epsilon^2\frac{\partial^2 w}{\partial z^2}\right), \quad (1)$$

$$\frac{\partial u}{\partial t}+\left[\frac{\partial}{\partial r}(u^2)+\frac{\partial}{\partial z}(uw)+\frac{u^2}{r}\right]\epsilon^8 = -\frac{1}{\epsilon^2}\frac{\partial p}{\partial r}+\frac{\epsilon^7}{Re}\left(\frac{\partial^2 u}{\partial r^2}+\frac{1}{r}\frac{\partial u}{\partial r}+\epsilon^2\frac{\partial^2 u}{\partial z^2}-\frac{u}{r^2}\right), \quad (2)$$

$$r\frac{\partial w}{\partial z}+\frac{\partial}{\partial r}(ur) = 0, \quad (3)$$

Notes

where r and z are the dimensionless coordinates scaled with respect to the radius of the unstented arterial lumen (a) and strut diameter (d) respectively while z-axis is located along the symmetry axis of the artery. The nondimensional components of the velocity along the axial and the radial directions are denoted by w and u respectively. The Reynolds number (Re) and the scaling parameter ϵ may be defined as $Re=\frac{\rho U_0 a}{\mu}$, $\epsilon=\frac{a}{d}$ where U_0 is the centreline velocity of the Poiseuille flow, ρ and μ are the density and the viscosity of the flowing blood respectively.

The unsteady convection-diffusion equation representing the transport of drug in the lumen may be written as

$$\frac{\partial c_f}{\partial t}+\left[\frac{\partial}{\partial r}(uc_f)+\frac{\partial}{\partial z}(wc_f)+\frac{uc_f}{r}\right]\epsilon^8 = \frac{\epsilon^7}{Pe_f}\left(\frac{\partial^2 c_f}{\partial r^2}+\frac{1}{r}\frac{\partial c_f}{\partial r}+\epsilon^2\frac{\partial^2 c_f}{\partial z^2}\right), \quad (4)$$

in which the luminal Peclet number $Pe_f=\frac{aU_0}{D_f}$; D_f, the drug diffusion coefficient in blood. Here c_f denotes the dimensionless luminal drug concentration.

Drug transport within the tissue has been represented by the unsteady diffusion process as

$$\frac{\partial c_t}{\partial t} = \frac{\epsilon^7}{Pe_t}\left(\frac{\partial^2 c_t}{\partial r^2}+\frac{1}{r}\frac{\partial c_t}{\partial r}+\epsilon^2\frac{\partial^2 c_t}{\partial z^2}\right), \quad (5)$$

where c_t is the dimensionless concentration of drug in the tissue and Pe_t $(=\frac{aU_0}{D_t})$ stands for the Peclet number in the tissue. Here D_t is the drug diffusion coefficient in the tissue.

In the lumen, symmetry boundary conditions were applied at the flow centreline:

$$\frac{\partial w}{\partial r}=0=u, \frac{\partial c_f}{\partial r}=0 \quad \text{on} \quad r=0. \quad (6)$$

No slip boundary condition have been imposed on lumen-strut (Γ_{bs}) and lumen-tissue (Γ_{bw}) interfaces:

$$w=0=u \quad \text{on} \quad r=R_b\ (=\Gamma_{bw}\cup\Gamma_{bs}). \quad (7)$$

Continuity of flux has been maintained at the lumen-tissue interface (Γ_{bw}) and release of drug from the struts has been simulated as a Dirichlet boundary condition with a drug concentration of unity at strut surfaces (Γ_{bs} and Γ_{ws}):

$$D_{f/t}\frac{\partial c_f}{\partial r}=\frac{\partial c_t}{\partial r} \quad \text{on} \quad \Gamma_{bw}, \quad (8)$$

$$c_f=1 \quad \text{on} \quad \Gamma_{bs}, \quad (9)$$

$$c_t=1 \quad \text{on} \quad \Gamma_{ws}, \quad (10)$$

where $D_{f/t}$ stands for the ratio of D_f and D_t.

A pulsatile velocity profile is imposed at the luminal inlet ($\Gamma_{b,in}$) [17]

$$w = (1 - \frac{r^2}{{R_b}^2})\bar{w}(t), u = 0 \quad \text{on} \quad \Gamma_{b,in}, \tag{11}$$

where $\bar{w}(t) = [1 + kcos(\epsilon^9 \frac{\alpha^2}{Re} t)]$, k is the dimensionless amplitude and $\alpha(= \sqrt{\frac{d^2\omega\rho}{\mu}})$ is the Womersley number in which ω is the frequency. Also, drug concentration was set to zero at the luminal inlet i.e.

$$c_f = 0 \quad \text{on} \quad \Gamma_{b,in}. \tag{12}$$

At the luminal outlet ($\Gamma_{b,out}$), zero velocity and concentration gradients are assumed:

$$\frac{\partial w}{\partial z} = 0 = \frac{\partial u}{\partial z} \quad \text{and} \quad \frac{\partial c_f}{\partial z} = 0 \text{ on } \Gamma_{b,out}. \tag{13}$$

In the tissue, symmetry boundary condition of drug transport are applied on the proximal ($\Gamma_{w,in}$) and the distal ($\Gamma_{w,out}$) walls:

$$\frac{\partial c_t}{\partial z} = 0 \quad \text{on} \quad \Gamma_{w,in} \text{ and } \Gamma_{w,out}. \tag{14}$$

A proper boundary condition at the perivascular wall (Γ_{wu}) is not apparent. Some researchers modelled it as a zero flux boundary condition [1, 19, 26], while some opted for a zero concentration boundary condition assuming the adventitia as a perfect sink [2, 15]. So instead of modelling a particular one, we investigate the effects of both the adventitial boundary conditions in this study:

$$\frac{\partial c_t}{\partial r} = 0 \quad \text{or} \quad c_t = 0 \text{ on } \Gamma_{wu}. \tag{15}$$

c) Solution procedure

In order to avoid interpolation error while discretising the governing equations, we transform the irregular (stented) domain into rectangular ones by making use of the following radial coordinate transformation:

$$\eta = \frac{r}{R_b} \quad , \quad \xi = 1 + \frac{r - R_{tl}}{R_{tu} - R_{tl}} = 1 + \frac{r - R_{tl}}{R}, \tag{16}$$

so that the arterial lumen transforms into a finite nondimensional rectangular domain as $[0, L] \times [0, 1]$, while the tissue domain into $[0, L] \times [1, 2]$. Here $R_b = \Gamma_{bw} \cup \Gamma_{bs}$, $R_{tl} = \Gamma_{bw} \cup \Gamma_{ws}$, $R_{tu} = \Gamma_{wu}$ and $R = R_{tu} - R_{tl}$. The transformed governing equations along with the set of boundary conditions are solved numerically by finite difference scheme in staggered grids. In this type of grid alignment, the velocities, the pressure and the drug concentrations are calculated in different locations of the control volume [cf. Figure 2]. The discretisation of the time-derivative terms is based on first order accurate two-level forward time-differentiating formula, while those for the convective terms in the momentum equations are accorded with a hybrid formula, consisting of central differencing and second order upwinding. The diffusive terms are, however, discretised by second order accurate central difference formula. The discretised equations are then solved by MAC method primarily introduced by Harlow and Welch [10]. Each run takes about 9 hours of CPU time in Debian Lenny 64-bit OS on a desktop of intel (R) core (TM) i5 with 8 GB RAM, for steady state computation. No standard package has been used in the present computations. However, our in-house code using FORTRAN language is based on the following computational sequences:

Ref

10. Harlow FH, Welch JE (1965) Numerical calculation of time-273 dependent viscous incompressible flow of fluid with free surface. Physics of Fluids 8:2182

Stage 1:

(i) $w^n_{i+\frac{1}{2},j}$, $u^n_{i,j+\frac{1}{2}}$, $c^n_{f_{i,j}}$ and $c^n_{t_{i,k}}$ are initialised at each cell (i, j). This is done either from result of the previous cycle or from the prescribed initial conditions.

(ii) Time step δt calculated from stability criteria.

(iii) The Poisson equation for pressure is solved to get the intermediate pressure-field $p^*_{i,j}$ using velocities $w^n_{i+\frac{1}{2},j}$, $u^n_{i,j+\frac{1}{2}}$ of the n^{th} time step.

(iv) The momentum equations are solved to get intermediate velocities $w^*_{i+\frac{1}{2},j}$, $u^*_{i,j+\frac{1}{2}}$ in an explicit manner using the previously known velocities and pressure.

Stage 2:

(v) The maximum cell divergence of velocity-field is calculated and checked for its tolerance. If the tolerance limit is satisfied, then drug transport equations are solved to get drug concentrations $c^{n+1}_{f_{i,j}}$ and $c^{n+1}_{t_{i,k}}$ in an explicit manner and steady-state convergence is checked for whether to stop calculation. If the maximum divergence of the velocity-field is found to be greater than the tolerance limit at any cell in absolute sense, go to step (vi).

(vi) The pressure at each cell is corrected to obtain $p^n_{i,j}$ and consequently the velocities at each cell are adjusted to get $w^{n+1}_{i+\frac{1}{2},j}$ and $u^{n+1}_{i,j+\frac{1}{2}}$. Then step (v) is again performed. This completes the necessary calculations for advancing flow-field through one cycle in time.

The process is to be repeated until steady-state convergence is achieved. Intersested readers are referred to Mandal et al. [19] for detailed discussion on method of solution, pressure-velocity correction and numerical stability.

III. Result and Discussion

For the purpose of numerical computation of the desired quantities of major physiological significance, the computational domain has been confined with a finite non-dimensional arterial length of 15. For this computational domain, solutions are computed through the generation of staggered grids with a size of 301×81 for both the lumen and the tissue regions. The simulation concerning the grid independence study was performed for the purpose of examining the error associated with the grid sizes used and is depicted in Figure 3. One may notice from this figure that the profiles concerning three distinct grid sizes almost overlap with one another for $Re = 500$ and $\alpha = 1$ in case of pulsatile inlet profile of the flowing blood. Thus the grid independence study in the present context of numerical simulation has its own importance to establish the correctness of the results obtained.

The variations of the dimensionless wall shear stress (WSS) distribution over the entire arterial segment having a pair of half–embedded DES^s in its lumen for different Reynolds numbers are exhibited in Figure 4. The flow separation points are observed when the WSS changes its sign. The reattachment points occur when the WSS changes its sign again. The curves in this figure show several flow separation zones from proximal and distal to the struts, where the latter is significantly larger than the former. One may note that the downstream separation length increases with increasing Reynolds numbers and the WSS gets its maximum value at the maximum height of the strut which also increases with increasing Reynolds numbers. Our simulations predict that these recirculation zones create pockets of stagnant drug–laden blood that allow drug accumulation at lumen-tissue interface and eventually filtration into the arterial wall. This observation is in conformity to that of Balakrishnan et al. [1] though they studied the transport of drug eluted from single and overlapping well-apposed DES^s in which the cross-section of the strut is square in shape.

Ref

1. Balakrishnan B, Tzafriri AR, Seifert P, Groothuis A, Rogers C, Edelman ER (2005) Strut position, blood flow, and drug deposition implications for single and overlapping drug-eluting stents. Circulation 111:2958–2965.

Figure 5(a) exhibits the profiles for the dimensionless drug concentration through the depth of the arterial tissue at $Pe_t = 1000, \alpha = 1$ and $Re = 500$ for different times. Here, drug concentration does increase with increasing time and thereafter, attains steady state for zero flux perivascular boundary condition. It is also to be observed that the penetration depth of drug within the tissue increases with increasing time. However, if one assumes zero concentration boundary condition at the perivascular end, the mean concentration appears to be much lower as compared to zero flux perivascular boundary condition [cf. Figure 5(b)].

Figures 6(a) and 6(b) show how the flow pulsatility affects the respective drug concentrations in both the lumen and the tissue at a depth of 1.5 strut radius for $Pe_f = 100, Pe_t = 1000, Re = 500$ and $\alpha = 1$. Both the figures reveal asymmetry between regions distal and proximal to the strut in which the degree of asymmetry appears to be much higher in the luminal concentration profile than that of the concentration profile within the tissue. The above observations may be argued in the sense that the asymmetry in the lumen is due to the convective nature of the luminal drug transport, however asymmetry in the tissue is due to stagnant drug–laden blood at the recirculation regions that allows drug accumulation and finally filtration beneath these regions. One more interesting observation is to be noted that the concentration of drug in both the lumen and the tissue is higher in case of usual parabolic inlet profile than that of the pulsatile one. Thus flow pulsatility significantly affects the transport of drug eluted from DES.

Figure 7(a) shows a change in Re of the flow alters the distribution of drug in the lumen while Figure 7(b) depicts that the mean drug uptake within the tissue is significantly affected by Re. Our simulation demonstrates that a decrease in concentration in the lumen with an increasing Re i.e. an inverse relationship between drug concentration and Re is revealed. A similar pattern is also observed in the tissue [cf. figure 7(b)]. The above observations may be justified in the sense that as Re increases, recirculation regions adjacent to the struts increase, which in turn, dilute the surface concentration of the pooling drug and decrease its contribution to the total drug deposition. Our observations are in good agreement with those of Kolachalama et al. [15] and O'Brien et al. [26].

Axial variation of drug concentration eluted from a pair of half–embedded DES^s with varying flow pulsatility (Womersley number) in the lumen is displaced in Figure 8(a). Our results reveal a complex interplay between Womersley number and arterial drug distribution. Evidently, an increase in vessel Womersley number via a change in the inlet flow profile is to increase the deposition in the lumen. It may also be noted that the mean concentration in the tissue does increase with increasing Womersley number [cf. Figure 8(b)], therefore, highlighting the importance of pulsatile inlet on stent-based drug delivery.

Figure 9 shows the concentration profile at a height 1.5 strut radius depending on interstrut distance for $Pe_f = 100, Pet = 1000, Re = 500$ and $\alpha = 1$. A single peak profile is noted when the struts are placed one strut radius apart. As the interstrut distance increases, the peak concentration falls and distinct peaks over each strut are observed. The spatial patterns for drug concentration [cf. Figures 10(a,b)] clearly establish our findings further. All these observations are in conformity to the findings of Balakrishnan et al. [1].

IV. Conclusion and Future Work

In this numerical investigation, we propose a two-dimensional axi-symmetric model of drug transport and luminal flow in presence of a pair of half-embedded DES^s. The finite-difference method used in this paper allows us to numerically solve the governing equations both in the lumen and the tissue. The present results predict a single peak profile when the struts

Ref

15. Kolachalama VB, Tzafriri AR, Arifin DY, Edelman ER (2009) Luminal flow patterns dictate arterial drug deposition in stent-based delivery. Journal of Controlled Release 133:24–30

are placed one strut radius apart and also as the interstrut distance increases, distinct peaks form over each strut. This study also highlights the facts that the mean concentration of drug within the tissue to be higher if one assumes the zero flux boundary condition instead of sink condition at the perivascular end. Another important observations may also be noted that as the Reynolds number increases, the drug concentration both in the lumen and the tissue decreases; however, a reverse trend is observed while changing the Womersley number. Though experimental studies can provide information on release kinetics and other histological information, computational studies can provide detailed predictions of the drug distribution over time. With the rapid ascent of stent–based drug delivery in the treatment of vascular disease, many important issues concerning drug delivery and its retention in the arterial tissue need to be addressed. The work presented in this paper only consider free drug as part of the governing equations. In reality, specific binding to tissue ultrastructural elements determines long term drug retention. As the target zone for stent-based delivery is atherosceloretic plaque [23], future direction for this work may also include different compositions of the plaque with varying diffusivity together with the time-dependent release kinetics.

V. Acknowledgement

The authors gratefully acknowledge the partial financial support from Special Assistance Programme (SAP-III) sponsored by University Grants Commission, New Delhi, India (Grant No- F.510/3/DRS-III/2015 (SAP-III)).

References Références Referencias

1. Balakrishnan B, Tzafriri AR, Seifert P, Groothuis A, Rogers C, Edelman ER (2005) Strut position, blood flow, and drug deposition implications for single and overlapping drug-eluting stents. Circulation 111:2958–2965.
2. Bozsak F, Chomaz JM, Barakat AI (2014) Modeling the transport of drugs eluted from stents: physical phenomena driving drug distribution in the arterial wall. Biomechanics and Modeling in Mechanobiology 13:327–347
3. Bozsak F, Gonzalez-Rodriguez D, Sternberger Z, Belitz P, Bewley T, Chomaz JM, Barakat AI (2015) Optimization of drug delivery by drug-eluting stents. PloS One 10(6):e0130,182, DOI 10.1371/journal.pone.0130182
4. Chen Y, Xiong Y, Jiang W,Wong MS, Yan F,Wang Q, Fan Y (2016) Numerical simulation on the effects of drug-eluting stents with different bending angles on hemodynamics and drug distribution. Medical and Biological Engineering and Computing pp 1–12
5. Chesnutt JK, Han HC (2015) Simulation of the microscopic process during initiation of stent thrombosis. Computers in Biology and Medicine 56:182–191
6. Fattori R, Piva T (2003) Drug-eluting stents in vascular intervention. The Lancet 361:247–249
7. Gogineni A, Ravigururajan T (2014) Flow through coated and non-coated coronary stented arteries: an overview. International Journal of Biomedical Engineering and Technology 14:344–367.
8. Grassi M, Pontrelli G, Teresi L, Grassi G, Comel L, Ferluga A, Galasso L (2009) Novel design of drug delivery in stented arteries: a numerical comparative study. Mathematical Biosciences and Engineering 6:493–508
9. Hajiali Z, Dabagh M, Debusschere N, De Beule M, Jalali P (2015) Tissue prolapse and stresses in stented coronary arteries: A computer model for multi-layer atherosclerotic plaque. Computers in Biology and Medicine 66:39–46.

Ref

23. McKittrick C, Kennedy S, Oldroyd K, McGinty S, McCormick C (2016) Modelling the impact of atherosclerosis on drug release and distribution from coronary stents. Annals of Biomedical Engineering 44:477–487

10. Harlow FH, Welch JE (1965) Numerical calculation of time-dependent viscous incompressible flow of fluid with free surface. Physics of Fluids 8:2182
11. Hill RA, Dündar Y, Bakhai A, Dickson R, Walley T (2004) Drug-eluting stents: an early systematic review to inform policy. European Heart Journal 25:902–919
12. Hwang CW, Wu D, Edelman ER (2001) Physiological transport forces govern drug distribution for stent-based delivery. Circulation 104:600–605
13. Inoue T, Croce K, Morooka T, Sakuma M, Node K, Simon DI (2011) Vascular inflammation and repair: implications for re-endothelialization, restenosis, and stent thrombosis. JACC: Cardiovascular Interventions 4:1057–1066
14. Kolachalama VB, Levine EG, Edelman ER (2009) Luminal flow amplifies stent-based drug deposition in arterial bifurcations. PloS One 4:e8105
15. Kolachalama VB, Tzafriri AR, Arifin DY, Edelman ER (2009) Luminal flow patterns dictate arterial drug deposition in stent-based delivery. Journal of Controlled Release 133:24–30
16. Koskinas KC, Chatzizisis YS, Antoniadis AP, Giannoglou GD (2012) Role of endothelial shear stress in stent restenosis and thrombosis: pathophysiologic mechanisms and implications for clinical translation. Journal of the American College of Cardiology 59:1337–1349
17. Lorenzini G, Casalena E (2008) CFD analysis of pulsatile blood flow in an atherosclerotic human artery with eccentric plaques. Journal of Biomechanics 41:1862–1870
18. Mandal AP, Mandal PK (2016) Drug elution model of coronary stent: effects of stent embedment and binding of drug. International Journal of Biomedical Engineering and Technology 20:150–165
19. Mandal AP, Sarifuddin, Mandal PK (2015) An unsteady analysis of arterial drug transport from half-embedded drug-eluting stent. Applied Mathematics and Computation 266:968–981
20. McGinty S, McKee S, Wadsworth RM, McCormick C (2011) Modelling drug-eluting stents. Mathematical Medicine and Biology 28:1–29
21. McGinty S, McKee S, McCormick C, Wheel M (2015) Release mechanism and parameter estimation in drug-eluting stent systems: analytical solutions of drug release and tissue transport. Mathematical Medicine and Biology 32:163–186
22. McHugh P, Barakat A, McGinty S (2016) Medical stents: State of the art and future directions. Annals of Biomedical Engineering 44:274–275
23. McKittrick C, Kennedy S, Oldroyd K, McGinty S, McCormick C (2016) Modelling the impact of atherosclerosis on drug release and distribution from coronary stents. Annals of Biomedical Engineering 44:477–487
24. Mongrain R, Leask R, Brunette J, Faik I, Bulman-Feleming N, Nguyen T (2004) Numerical modeling of coronary drug eluting stents. Studies in Health Technology and Informatics 113:443–458
25. Mongrain R, Faik I, Leask RL, Rod´s-Cabau J, Larose E, Bertrand OF (2007) Effects of diffusion coefficients and struts apposition using numerical simulations for drug eluting coronary stents. Journal of Biomechanical Engineering 129:733–742
26. O'Brien CC, Kolachalama VB, Barber TJ, Simmons A, Edelman ER (2013) Impact of flow pulsatility on arterial drug distribution in stent-based therapy. Journal of Controlled Release 168:115–124

Notes

27. Ponde CK, Aroney CN, McEniery PT, Bett JH (1997) Plaque prolapse between the struts of the intracoronary palmaz-schatz stent: Report of two cases with a novel treatment of this unusual problem. Catheterization and Cardiovascular Diagnosis 40:353–357
28. Pontrelli G, De Monte F (2007) Mass diffusion through two-layer porous media: an application to the drug-eluting stent. International Journal of Heat and Mass Transfer 50:3658–3669
29. Pontrelli G, De Monte F (2010) A multi-layer porous wall model for coronary drug eluting stents. International Journal of Heat and Mass Transfer 53:3629–3637
30. Prendergast P, Lally C, Daly S, Reid A, Lee T, Quinn D, Dolan F (2003) Analysis of prolapse in cardiovascular stents: a constitutive equation for vascular tissue and finite-element modelling. Journal of Biomechanical Engineering 125:692–699
31. Sarifuddin, Mandal PK (2016) Effect of diffusivity on the transport of drug eluted from drug-eluting stent. International Journal of Applied and Computational Mathematics 2:291–301
32. Tesfamariam B (2008) Drug release kinetics from stent device-based delivery systems. Journal of Cardiovascular Pharmacology 51:118–125
33. Vairo G, Cioffi M, Cottone R, Dubini G, Migliavacca F (2010) Drug release from coronary eluting stents: a multidomain approach. Journal of Biomechanics 43:1580–1589
34. Van Der Hoeven BL, Pires NM, Warda HM, Oemrawsingh PV, Van Vlijmen BJ, Quax PH, Schalij MJ, Van Der Wall EE, Jukema JW (2005) Drug-eluting stents: results, promises and problems. International Journal of Cardiology 99:9–17
35. Venkatraman S, Boey F (2007) Release profiles in drug-eluting stents: issues and uncertainties. Journal of Controlled Release 120:149–160
36. Zunino P, Tambaca J, Cutri E, Canic S, Formaggia L, Migliavacca F (2016) Integrated stent models based on dimension reduction: Review and future perspectives. Annals of Biomedical Engineering 44:604–617

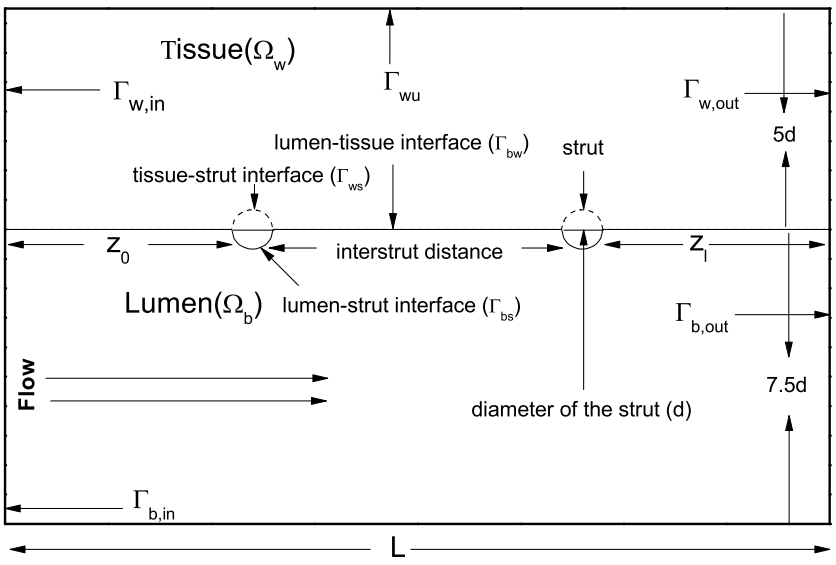

Figure 1: Schematic diagram of the stented artery

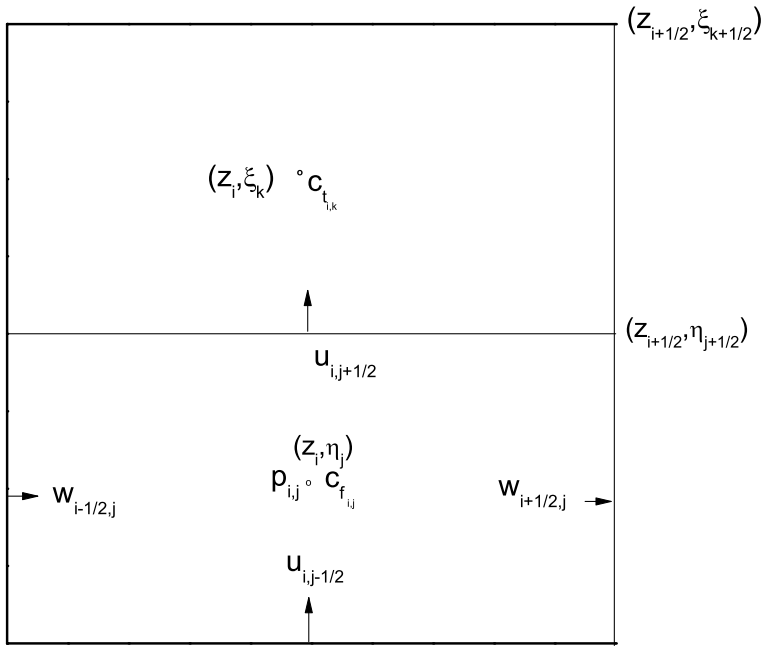

Figure 2: A typical combined MAC cell for lumen and tissue.

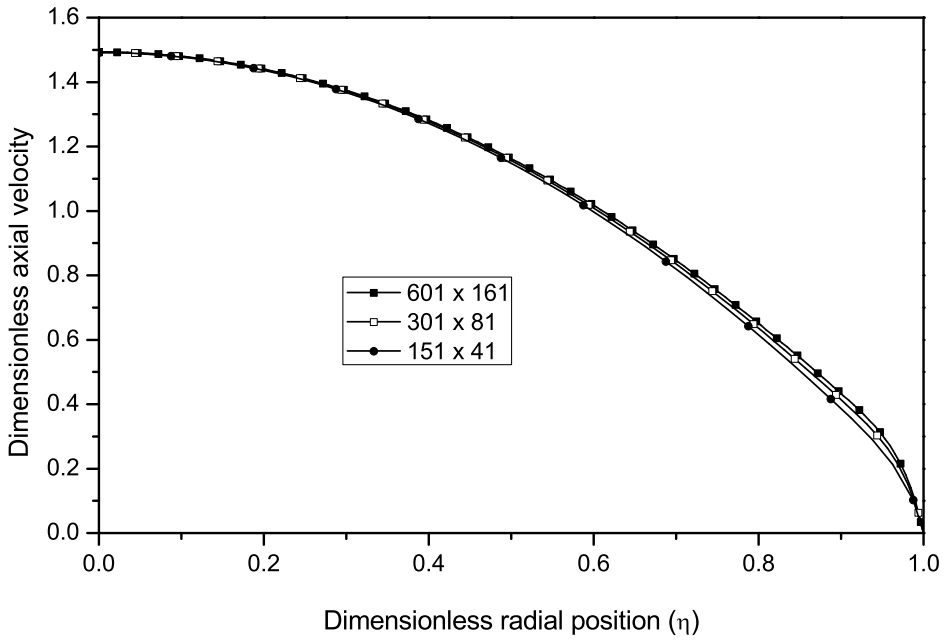

Figure 3: Dimensionless axial velocity profile at z=3.5 for different grid sizes (Re=500, α=1).

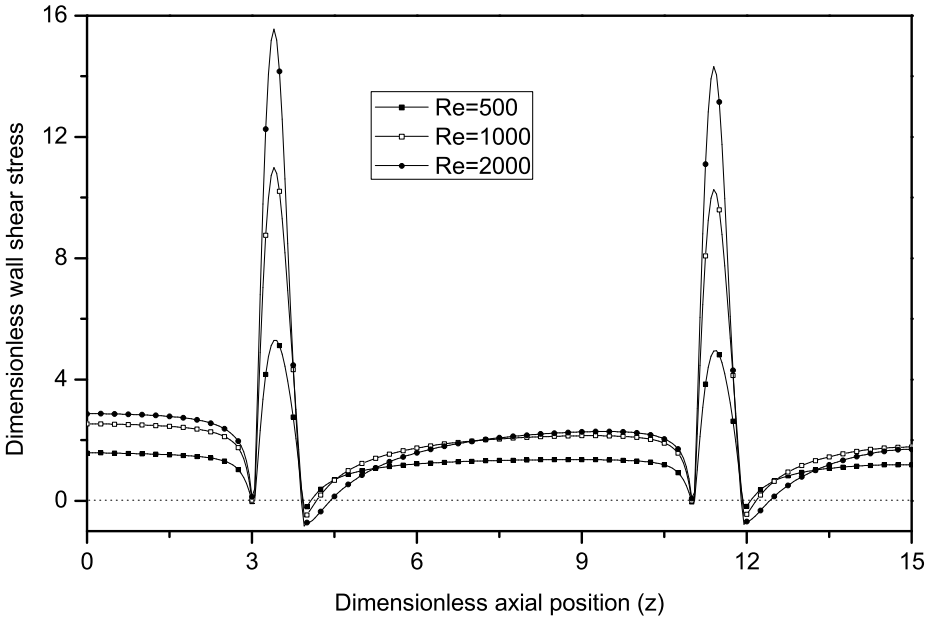

Figure 4: Distribution of dimensionless wall shear stress for different Reynlods numbers (α=1, Pe_f=100, Pe_t=1000).

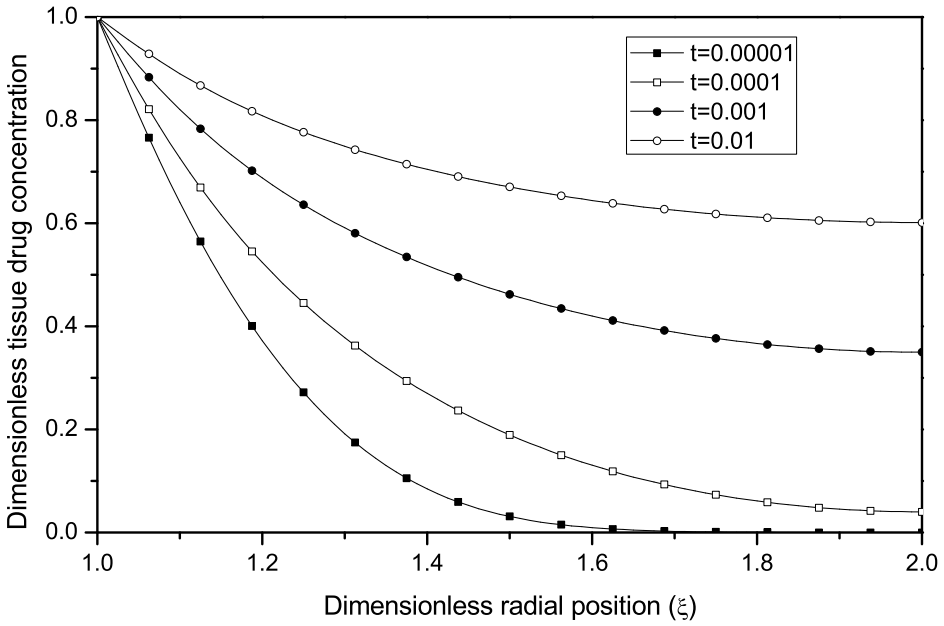

Figure 5(a): Transmural variation of dimensionless tissue drug concentration for different times (Pe_f=100, Pe_t=1000, Re=500, α=1).

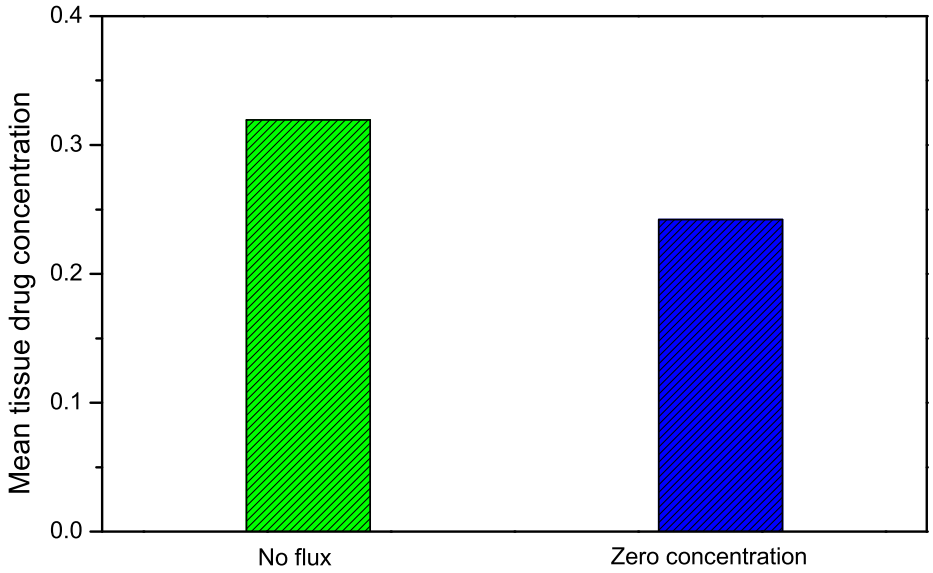

Figure 5(b): Mean concentration of drug within the tissue for different perivascular boundary conditions (Re=500, Pe_f=100, Pe_t=1000, α=1)

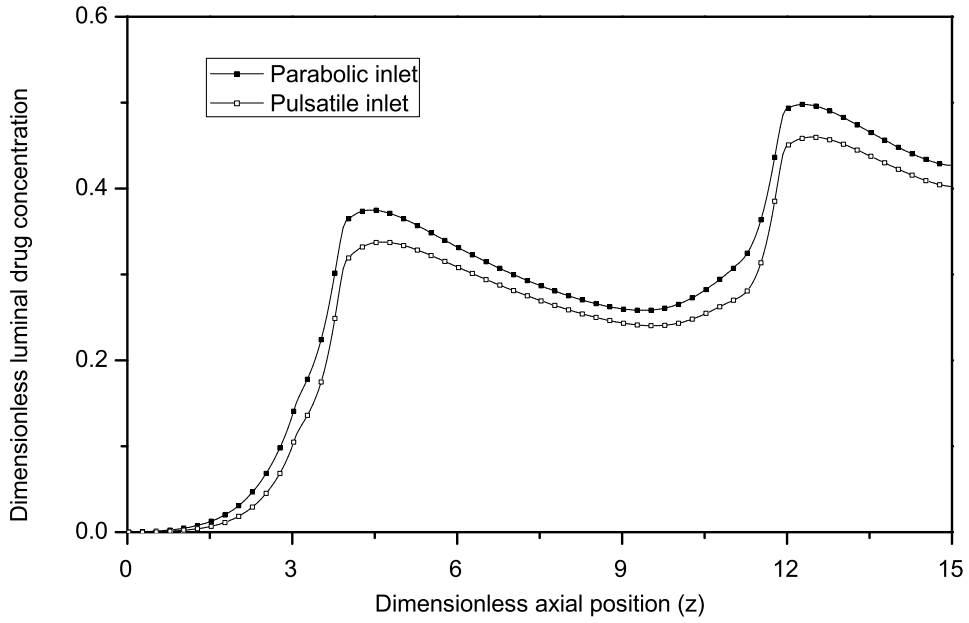

Figure 6(a): Axial variation of luminal drug concentration at a depth of 1.5 strut radius from mural interface for different types of inlet flow (Pe_f=100, Pe_t=1000, Re=500, α=1)

Notes

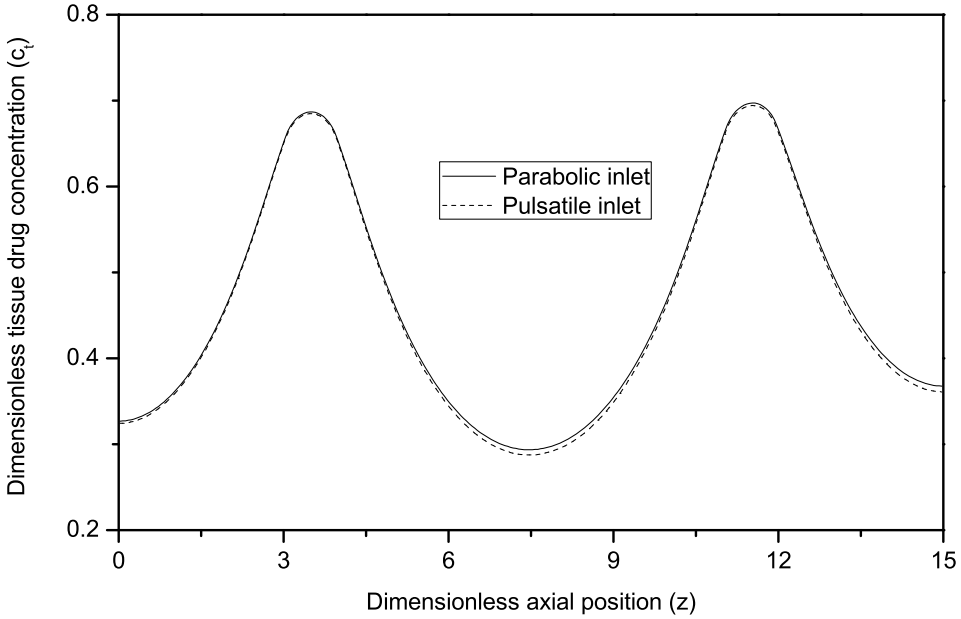

Figure 6(b): Axial variation of tissue drug concentration at a height of 1.5 strut radius from mural interface for different types of inlet flow (Pe_f=100, Pe_t=1000, Re=500, α=1)

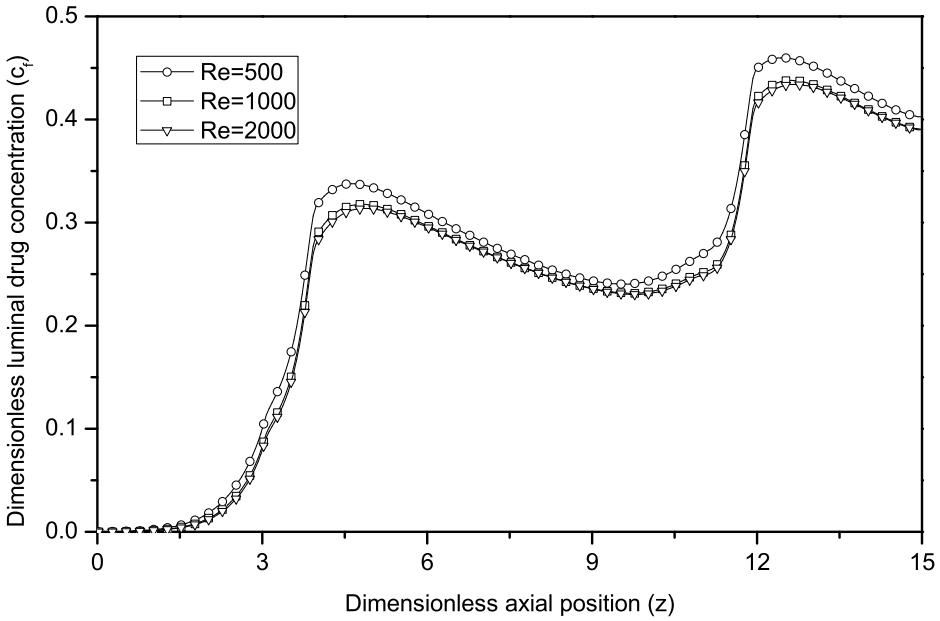

Figure 7(a): Axial variation of luminal drug concentration at a depth of 1.5 strut radius for different Reynolds numbers (Pef=100, Pet=1000, α=1)

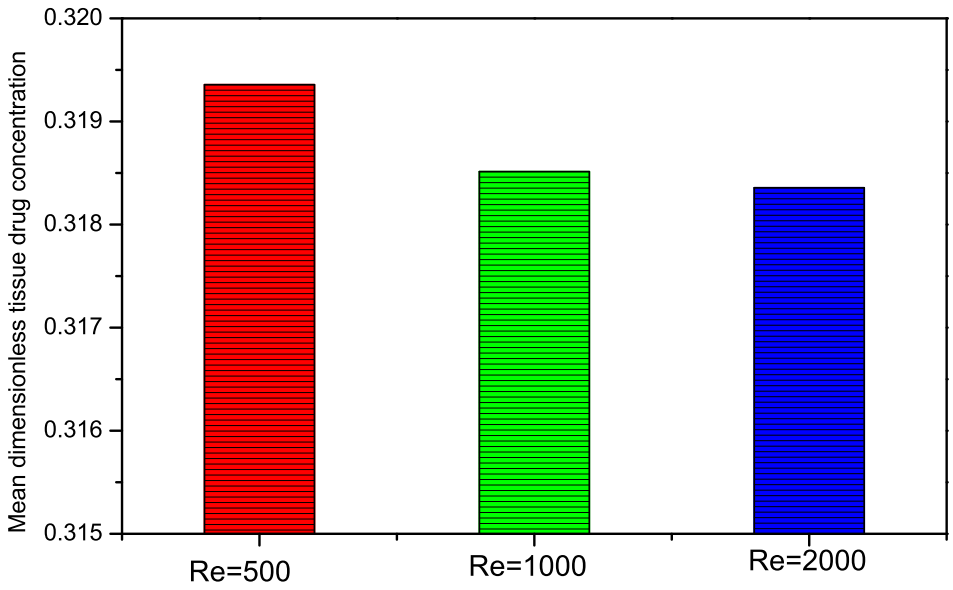

Figure 7(b): Mean drug concentration in the tissue for different Reynolds numbers (Pe_f=100, Pe_t=1000, α=1)

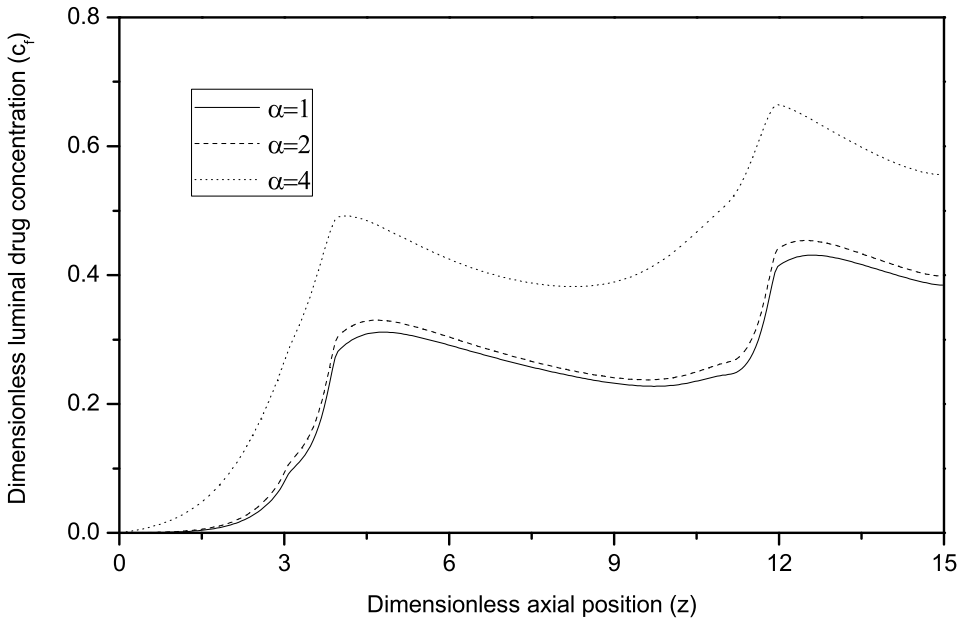

Figure 8(a): Axial variation of luminal drug concentration at a depth of 1.5 strut radius for different Womersley numbers (Re=500, Pe_f=100, Pe_t=1000)

Notes

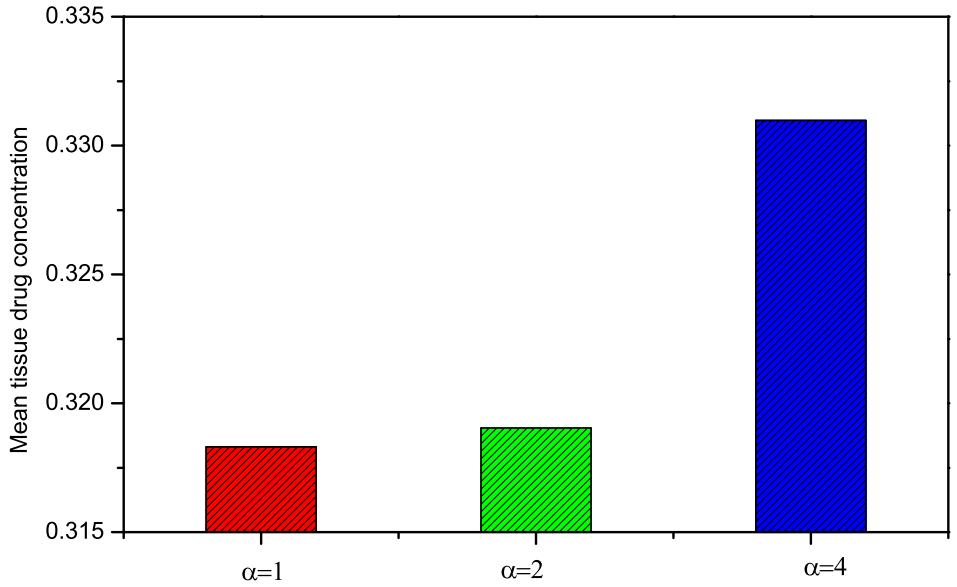

Figure 8(b): Mean tissue drug concentration in the tissue for different Womersley numbers (Pe_f=100, Pe_t=1000, Re=500)

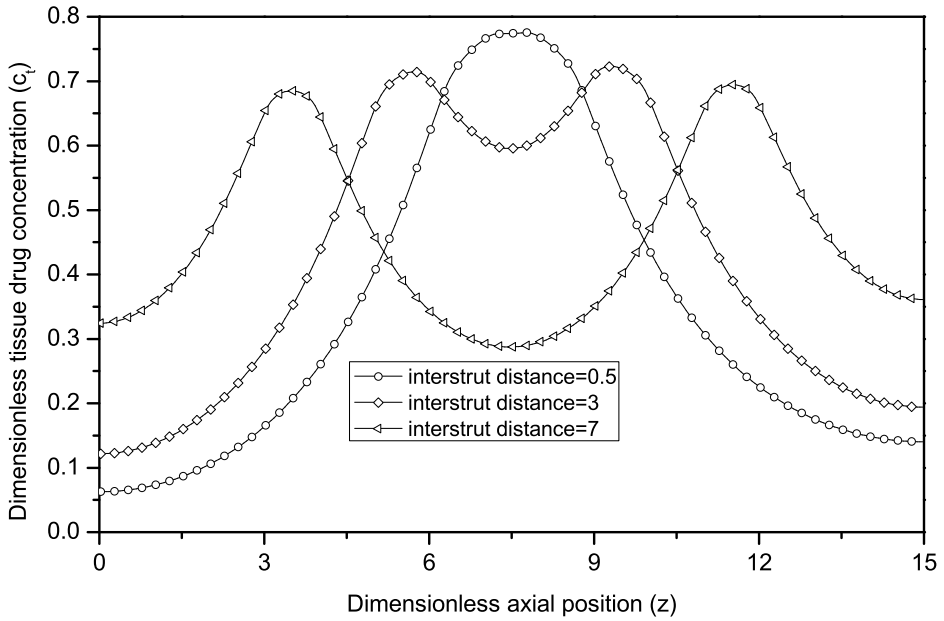

Figure 9: Axial variation of tissue drug concentration at a height of 1.5 strut radius in the tissue (Pe_f=100, Pe_t=1000, Re=500, α=1)

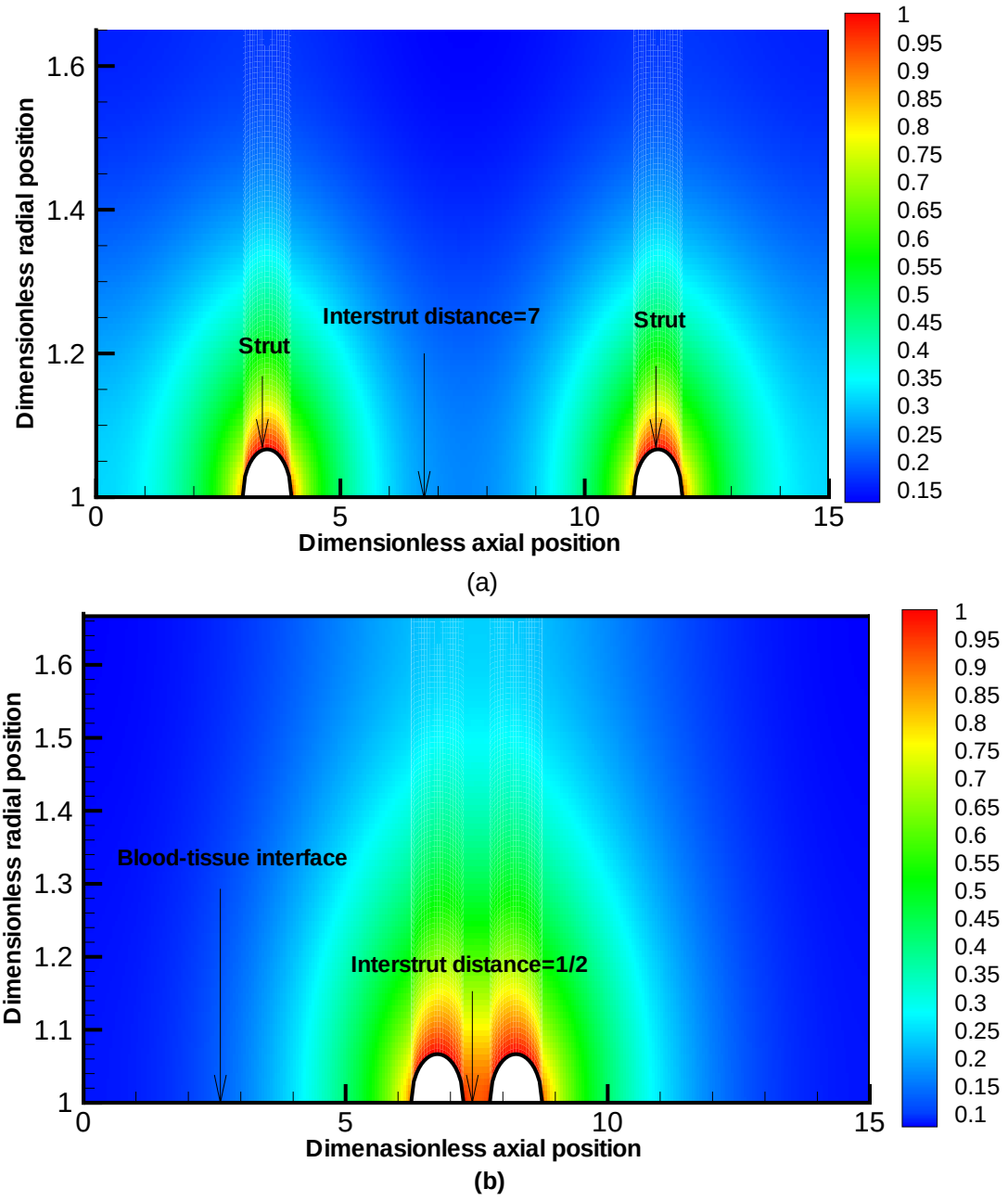

Figure 10: Visual representation of drug concentration in the tissue, (a) interstrut distance=7, (b) interstrut distance=1/2 (Re=500, Pe_f =100, Pe_t =1000, α=1)

Notes